The Astrophysical Journal, 609:962–971, 2004 July 10

ON THE AFTERGLOW OF THE X-RAY FLASH OF 2003 JULY 23: PHOTOMETRIC EVIDENCE FOR AN OFF-AXIS GAMMA-RAY BURST WITH AN ASSOCIATED SUPERNOVA?[1]

J. P. U. Fynbo,[2,3] J. Sollerman,[4] J. Hjorth,[3] F. Grundahl,[2,3] J. Gorosabel,[5,6] M. Weidinger,[2,7] P. Møller,[7] B. L. Jensen,[3] P. M. Vreeswijk,[8] C. Fransson,[4] E. Ramirez-Ruiz,[9] P. Jakobsson,[3] S. F. Jørgensen,[3] C. Vinter,[3] M. I. Andersen,[10] J. M. Castro Cerón,[6] A. J. Castro-Tirado,[5] A. S. Fruchter,[6] J. Greiner,[11] C. Kouveliotou,[12] A. Levan,[13] S. Klose,[14] N. Masetti,[15] H. Pedersen,[3] E. Palazzi,[16] E. Pian,[17,17] J. Rhoads,[6] E. Rol,[15] T. Sekiguchi,[18] N. R. Tanvir,[19] P. Tristram,[20] A. de Ugarte Postigo,[6] R. A. M. J. Wijers,[15] and E. van den Heuvel[15]

Received 2004 February 11; accepted 2004 March 23

ABSTRACT

We present optical and near-infrared follow-up observations of the X-ray flash (XRF) of 2003 July 23. Our observations in the *R* band cover the temporal range from 4.2 hr to 64 days after the high-energy event. We also present the results of multicolor imaging extending to the *K* band on three epochs. The light curve of the *R*-band afterglow the first week after the burst is similar to the light curve for long-duration gamma-ray bursts (GRBs), i.e., a broken power law with a late time slope of $\alpha \approx 2.0$ ($F_\nu \propto t^{-\alpha}$). Furthermore, the spectral energy distribution (SED) has a power-law ($F_\nu \propto \nu^{-\beta}$) shape with slope $\beta \approx 1.0$. However, the decay slope at $t < 1$ day is shallow, consistent with zero. This is in qualitative agreement with the prediction that XRFs are off-axis classical GRBs. After the first week there is a strong bump in the light curve, which peaks at around 16 days. The SED after the peak becomes significantly redder. We discuss the possible interpretations of this bump and conclude that an underlying supernova is the most likely explanation since no other model appears consistent with the evolution of the SED. Finally, we present deep spectroscopy of the burst both in the afterglow and in the bump phase. A firm upper limit of $z = 2.3$ is placed on the redshift of XRF 030723 from the lack of Lyα forest lines in the spectrum of the afterglow. The lack of significant absorption and emission lines in either of the two spectra excludes a spectroscopic redshift determination.

Subject headings: cosmology: observations — gamma rays: bursts — supernovae: general — X-rays: individual (XRF 030723)

1. INTRODUCTION

X-ray flashes (XRFs) are transient sources of X-ray photons that are distributed isotropically on the sky. Their existence as a class with a different nature than X-ray bursters in the Galaxy was first put forward by Heise et al. (2001) based on data from the *BeppoSAX* satellite. They introduced an operational definition for XRFs, namely, a fast transient source with duration less than 1000 s in the Wide Field Camera (covering 2–25 keV) that did not trigger the Gamma Ray Burst Monitor (covering 40–700 keV). *BeppoSAX* detected 20 such events in the 6 yr it was operational (Heise et al. 2003). A *HETE-2* burst is classified as an XRF if its X-ray fluence (S) exceeds its gamma-ray fluence, i.e., $\log[(02-30\ \mathrm{keV})/S(30-400\ \mathrm{keV})] > 0$ (Lamb et al. 2003). Classical gamma-ray bursts (GRBs) are defined as having $\log[S(2-30\ \mathrm{keV})/S(30-400\ \mathrm{keV})] < -0.5$, while bursts belonging to the intermediate class are classified as X-ray–rich GRBs, following Castro-Tirado et al. (1994).

XRFs can be interpreted as the same phenomenon as classical GRBs, with the difference being that the high-energy spectra for XRFs are softer than for GRBs (Heise et al. 2001; Barraud et al. 2003). The high-energy spectra (νF_ν) of GRBs are well described by the so-called Band function (Band et al. 1993), which is composed of two smoothly connected power laws. The energy at which the two power laws connect is

[1] Based on observations made with ESO Telescopes at the Paranal and La Silla Observatories under program ID 71.A-0355(A, B, C, F, G).

[2] Department of Physics and Astronomy, University of Aarhus, Ny Munkegade, DK-8000 Århus C, Denmark.
[3] Niels Bohr Institute, Astronomical Observatory, University of Copenhagen, Juliane Maries Vej 30, DK-2100 Copenhagen Ø, Denmark.
[4] Stockholm Observatory, Department of Astronomy, AlbaNova, S-106 91 Stockholm, Sweden.
[5] Instituto de Astrofísica de Andalucía (CSIC), c. Camino Bajo de Huétor, 24, E-18.008 Granada, Spain.
[6] Space Telescope Science Institute, 3700 San Martin Drive, Baltimore, MD 21218.
[7] European Southern Observatory, Karl Schwarzschild-Strasse 2, D-85748 Garching, Germany.
[8] European Southern Observatory, Alonso de Córdova 3107, Casilla 19001, Santiago 19, Chile.
[9] School of Natural Sciences, Institute for Advanced Study, Einstein Drive, Princeton, NJ 08540; Chandra Fellow.
[10] Astrophysikalisches Institut Potsdam, An der Sternwarte 16, D-14482 Potsdam, Germany.
[11] Max-Planck-Institute for Extraterrestrial Physics, D-85741 Garching, Germany.
[12] Universities Research Association, Marshall Space Flight Center (NASA), Huntsville, AL 35812.
[13] X-ray Astronomy Group, Department of Physics and Astronomy, Leicester University, Leicester LE1 7RH, UK.
[14] Thüringer Landessternwarte Tautenburg, D-07778 Tautenburg, Germany.
[15] IASF/CNR, Sezione di Bologna, Via Gobetti 101, I-40129 Bologna, Italy.
[16] INAF, Osservatorio Astronomico di Trieste, via Tiepolo, I-34131 Trieste, Italy.
[17] Astronomical Institute 'Anton Pannekoek,' NL-1098 SJ Amsterdam, The Netherlands.
[18] Solar Terrestrial Environment Laboratory, Nagoya University, Nagoya 464-8601, Japan.
[19] Department of Physical Sciences, University of Hertfordshire, College Lane, Hatfield, Hertfordshire AL10 9AB, UK.
[20] Canterbury University's Mt John Observatory, Lake Tekapo, New Zealand.

referred to as $E_{\rm peak}$ and is where most of the energy usually is emitted. For classical GRBs $E_{\rm peak}$ is typically a few 100 keV (Preece et al. 2000). The high-energy spectra of XRFs are also well fitted by the Band function, but with values of $E_{\rm peak}$ below 100 keV and in some cases even below 10 keV (Kippen et al. 2002; Barraud et al. 2003). For classical GRBs there is a correlation between spectral hardness, defined as the fluence in the X-ray band divided by the fluence in the gamma-ray band, and the fluence in the gamma-ray band in the sense that hard bursts have a higher total fluence Nemiroff et al. 1994. XRFs follow this correlation Barraud et al. 2003. These properties of GRBs and XRFs would be naturally explained if XRFs were GRBs at very large redshifts. However, the lack of excessive time dilation compared to GRBs argues against this interpretation (Heise et al. 2001). Moreover, Amati et al. (2002) find in a sample of 12 *BeppoSAX* GRBs with known redshifts that the total isotropic equivalent energy radiated in the 1–10,000 keV range is positively correlated with $E_{\rm peak}$. This also argues against very large redshifts for XRFs. Instead, the current view is that XRFs are the result of either (1) classical GRBs seen off-axis (Yamazaki et al. 2002, 2003; Dado et al. 2003; Rhoads 2003), (2) so-called dirty fireballs, which are relativistic jets with a larger baryon load and hence (assuming external shocks) lower Γ-factor than those of classical GRBs (Dermer et al. 1999; Heise et al. 2001), or (3) fireballs with large Γ-factors and/or low baryon loading that in the case of internal shocks lead to the emission of less energetic photons (Zhang & Mészáros 2002; Barraud et al. 2003).

Prior to XRF 030723, four XRFs had been localized to arcminute accuracy. The first was the *BeppoSAX* burst XRF 011030 (e.g., Heise et al. 2001), for which a likely afterglow was detected at radio (Taylor et al. 2001) and X-ray wavelengths (Harrison et al. 2001). The first XRF localized by *HETE-2* (XRF 011130) did not lead to an unambiguous afterglow detection despite extensive efforts at optical, X-ray and, radio wavelengths. XRF 020427, localized by *BeppoSAX*, exhibited an X-ray afterglow, localized to arcsecond accuracy by the *Chandra X-Ray Observatory* (Fox 2002). The first *HETE-2* XRF for which an afterglow was identified was XRF 020903 (Ricker et al. 2002). A candidate optical and radio afterglow was detected and a bright galaxy coincident with the transient was found at $z = 0.251$ (Soderberg et al. 2003b). Finally, Watson et al. (2004) suggest that the *Integral* burst GRB 031203 was actually an XRF on the basis of the modeling of a dust echo in our galaxy observed by *XMM* (Vaughan et al. 2004). For GRB 031203 a radio afterglow (Frail 2003), but no optical afterglow, has been detected. The likely redshift of this burst is only 0.105, based on the spectrum of a galaxy coincident with the position of the radio afterglow (Prochaska et al. 2004).

Hubble Space Telescope (*HST*) observations have been obtained of the fields of XRF 011030, 020903, and 020427. In all cases a candidate host galaxy has been identified. XRFs 011030 and 020427 exhibited blue $R \sim 24$ host galaxies, typical of GRB host galaxies (Bloom et al. 2003). The galaxies are probably not at a very high redshift ($z \leq 3.5$; Bloom et al. 2003). The host galaxy of XRF 020903 exhibits a complex morphology (Levan et al. 2002; Soderberg et al. 2003b). A single emission line at 8485 Å has been detected from the host galaxy of XRF 020427 (van Dokkum & Bloom 2003).

XRF 030723 was detected by the FREGATE, WXM, and SXC instruments on board the *HETE-2* satellite on 2003 July 23.26965 UTC (*HETE* trigger H2777). The event was localized with the SXC to a $2'$ radius error circle at high Galactic latitude ($b = 50^\circ$) in the constellation Pisces Aus Prigozhin et al. 2003. The burst duration (T_{90}) was 25 s. The total fluence in the 7–30 keV band was $\sim 2 \times 10^{-7}$ ergs cm^{-2}, and in the 30–400 keV band the fluence was less than 7×10^{-8} ergs cm^{-2}. It was hence clearly an XRF according to the *HETE-2* definition. Observations of the X-ray afterglow to XRF 030723 has been reported by Butler et al. (2004). In the radio band only an upper limit of 180 μJy at 8.46 GHz (July 26.42 UT) has been reported (Soderberg et al. 2003a). In this paper we present a comprehensive optical and near-infrared (near-IR) study of its afterglow—the first such study for any XRF.

2. OBSERVATIONS

We initiated optical follow-up observations of the SXC error box 4.2 hr after the flash. This was done near morning twilight from the Danish 1.5 m Telescope (D1.5m) at ESO's La Silla Observatory. Based on these observations we flagged the object later found to be the optical afterglow as the brightest source ($R = 20.9$) not present in the Digitized Sky Survey. Images were secured at the D1.5m also on the following night to facilitate detection of the afterglow as a transient source. Comparison of the images from the first and second epoch observations revealed no apparent transients in the error box (Jensen et al. 2003). This later turned out to be due to the small initial variability of the afterglow: within the errors the afterglow had the same *R*-band magnitude 4.2 and 21.0 hr after the burst. The detection of the optical afterglow was subsequently reported by Fox et al. (2003). The fact that we had observed an initially flat light curve suggested to us that XRF 030723 was an off-axis GRB. Off-axis bursts should be observable only to modest redshifts (Yamazaki et al. 2002), and we therefore decided to conduct a targeted effort at detecting emission from the expected associated supernova (Stanek et al. 2003; Hjorth et al. 2003a). We continued to observe the afterglow at optical and near-IR wavelengths for the following 64 days using the D1.5m and ESO telescopes at the La Silla and Paranal observatories. The afterglow was also observed at 8.1 hr after the burst with the 0.6 m telescope on Mount John in New Zealand in wide MOA (Microlensing Observations in Astrophysics) *RI*-, and *BV*-band filters. The full journal of observations is given in Table 1. The data were reduced using standard techniques for debiasing and flat-fielding.

3. RESULTS

3.1. *Astrometry*

We have determined the celestial position of the optical afterglow by comparison with nine stars from the Two Micron All Sky Survey (2MASS) catalog. We find the position R.A. $= 21^{\rm h}49^{\rm m}24^{\rm s}.42$, decl. $= -27^\circ 42'' 47''.30$ (J2000.0) within an rms scatter of $0''.06$. The 2MASS astrometry is tied to the International Celestial Reference System (ICRS) via the Tycho 2 Catalog and is accurate to 70–80 mas. The position we derive is consistent with the position reported by Fox et al. (2003).

3.2. *The Light Curve*

The optical photometry of the XRF was carried out using the DAOPHOT/ALLSTAR/ALLFRAME photometry packages developed by Stetson (1987, 1994). Initially each image

TABLE 1

LOG OF OBSERVATIONS AND PHOTOMETRY OF THE AFTERGLOW OF XRF 030723

Date (UT)	Δt (days)	Filter/Grism	Exposure Time (s)	Instrument	Brightness (mag)
Jul 23.44329.....	0.1736	R	300	D1.5m/DFOSC	20.92 ± 0.11
Jul 23.6090.....	0.3394	BV-MOA	3×300	0.6m/MOA	21.47 ± 0.25
Jul 23.6090.....	0.3394	RI-MOA	3×300	0.6m/MOA	>20.9
Jul 24.133.....	0.863	R	3×600	D1.5m/DFOSC	20.98 ± 0.05
Jul 24.333.....	1.063	R	3×600	D1.5m/DFOSC	21.15 ± 0.05
Jul 24.360.....	1.090	V	3×600	D1.5m/DFOSC	21.63 ± 0.03
Jul 24.384.....	1.114	J_s	15×60	NTT/SOFI	19.81 ± 0.06
Jul 24.397.....	1.127	H	15×60	NTT/SOFI	19.14 ± 0.11
Jul 24.409.....	1.139	K_s	15×60	NTT/SOFI	18.33 ± 0.06
Jul 24.421.....	1.151	J_s	15×60	NTT/SOFI	19.79 ± 0.08
Jul 24.433.....	1.163	H	15×60	NTT/SOFI	19.26 ± 0.12
Jul 24.446.....	1.176	K_s	15×60	NTT/SOFI	18.42 ± 0.10
Jul 24.396.....	1.126	i	3×600	D1.5m/DFOSC	20.72 ± 0.04
Jul 24.411.....	1.141	R	4×600	D1.5m/DFOSC	21.24 ± 0.05
Jul 25.114.....	1.844	R	3×600	D1.5m/DFOSC	22.00 ± 0.10
Jul 25.346.....	2.076	R	7×600	D1.5m/DFOSC	22.31 ± 0.07
Jul 25.378.....	2.108	J_s	15×60	NTT/SOFI	20.14 ± 0.16
Jul 25.391.....	2.121	H	15×60	NTT/SOFI	19.50 ± 0.22
Jul 25.403.....	2.133	K_s	15×60	NTT/SOFI	19.08 ± 0.25
Jul 25.408.....	2.138	R	8×600	D1.5m/DFOSC	22.13 ± 0.05
Jul 26.236.....	2.966	V	50	VLT/FORS1	23.41 ± 0.07
Jul 26.239.....	2.969	V	50	VLT/FORS1	23.28 ± 0.07
Jul 26.33.....	3.06	G300V+GG375	22×600	VLT/FORS1	Spectra
Jul 27.160.....	3.890	K_s	10×60	VLT/ISAAC	21.04 ± 0.21
Jul 27.171.....	3.901	J_s	10×60	VLT/ISAAC	22.46 ± 0.23
Jul 27.180.....	3.910	H	10×60	VLT/ISAAC	21.06 ± 0.15
Jul 27.212.....	3.942	U	6×300	VLT/FORS1	23.83 ± 0.15
Jul 27.228.....	3.958	B	300	VLT/FORS1	24.31 ± 0.07
Jul 27.232.....	3.962	B	300	VLT/FORS1	24.57 ± 0.10
Jul 27.236.....	3.966	V	300	VLT/FORS1	24.04 ± 0.06
Jul 27.241.....	3.971	V	300	VLT/FORS1	24.12 ± 0.12
Jul 27.245.....	3.975	R	300	VLT/FORS1	23.64 ± 0.05
Jul 27.249.....	3.979	R	300	VLT/FORS1	23.56 ± 0.05
Jul 27.255.....	3.985	i	300	VLT/FORS1	23.08 ± 0.08
Jul 27.260.....	3.990	i	300	VLT/FORS1	23.08 ± 0.08
Jul 29.150.....	5.880	R	300	VLT/FORS1	24.63 ± 0.13
Jul 29.154.....	5.884	R	300	VLT/FORS1	24.38 ± 0.11
Jul 29.158.....	5.888	R	300	VLT/FORS1	24.62 ± 0.13
Jul 31.100.....	7.830	R	6×300	VLT/FORS2	25.00 ± 0.14
Aug 3.240	10.970	R	12×300	VLT/FORS2	25.16 ± 0.07
Aug 6.228	13.958	V	6×600	NTT/SUSI2	24.39 ± 0.08
Aug 6.240	13.970	i	6×600	NTT/SUSI2	23.92 ± 0.23
Aug 6.254	13.984	R	6×600	NTT/SUSI2	24.28 ± 0.07
Aug 6.308	14.038	R	6×600	VLT/FORS1	24.14 ± 0.03
Aug 6.368	14.098	B	6×600	NTT/SUSI2	25.04 ± 0.10
Aug 7.291	15.021	R	180	VLT/FORS2	24.16 ± 0.09
Aug 7.296	15.026	R	180	VLT/FORS2	24.20 ± 0.11
Aug 7.359	15.089	600RI+GG435	15×540	VLT/FORS2	Spectra
Aug 8.327	16.057	R	180	VLT/FORS2	24.04 ± 0.13
Aug 8.331	16.061	R	180	VLT/FORS2	24.03 ± 0.10
Aug 8.380	16.110	600RI+GG435	10×540	VLT/FORS2	Spectra
Aug 9.396	17.126	R	6×300	VLT/FORS2	24.16 ± 0.04
Aug 10.335	18.065	R	14×600	D1.5m/DFOSC	23.88 ± 0.44
Aug 14.168	21.898	K_s	150×60	VLT/ISAAC	21.19 ± 0.11
Aug 17.052	24.782	R	15×600	NTT/SUSI2	25.08 ± 0.09
Aug 19.007	26.737	B	3×600	VLT/FORS1	>26.8
Aug 19.091	26.821	U	15×600	VLT/FORS1	>27.0
Aug 19.168	26.898	R	3×600	VLT/FORS1	24.99 ± 0.06
Aug 19.191	26.921	i	3×600	VLT/FORS1	23.88 ± 0.05
Sep 3.291	42.021	R	6×600	VLT/FORS1	25.97 ± 0.12
Sep 25.135	63.865	R	$4 \times 600 + 480$	VLT/FORS1	26.58 ± 0.29

NOTE.—Upper limits are measured in a circular aperture with diameter of $2''$ and are $2\ \sigma$.

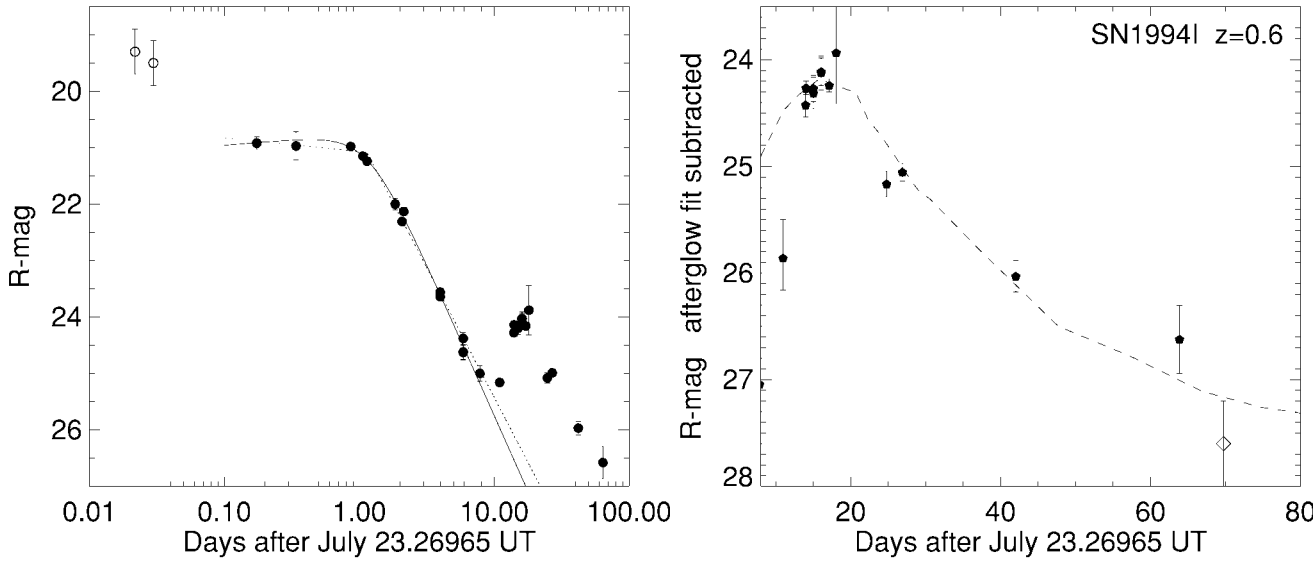

FIG. 1.—*Left:* The *R*-band light curve of the afterglow of XRF 030723. The filled circles are the measurements from this work (Table 1), and the two open circles are the tentative early detections from the ROTSE-III Telescope (Smith et al. 2003a). The dashed and solid lines are the result of broken power law and Beuermann function fit to the first 12 data points. *Right:* The late-time bump. In this plot we have subtracted the extrapolation of the power-law component from the afterglow (based on the Beuermann fit). The errors include the photometric error as well as the formal error from the subtraction of the Beuermann fit. We also include the latest reported detection (*open circle*) of Kawai et al. (2003). The dashed curve shows the *B*-band light curve of the Type Ic SN 1994I redshifted to $z = 0.6$, and scaled up in flux by 1 mag. This combination of redshift and a very fast light curve provides the best match to the late light curve.

was run through DAOPHOT and ALLSTAR to produce a point-spread function (PSF) and a star list. Subsequently *daomaster* and *daomatch* were used on the ALLSTAR photometry to derive positional transformations between the images and generate a master star list. From the master star list seven isolated objects were selected as PSF stars and then a new PSF was generated for each image using these stars. After this step, we obtained the final PSF photometry using the ALLFRAME program (Stetson 1994), with the PSFs and positional transformations generated above. The error bars reported on the photometry are those produced by ALLFRAME. The relative magnitudes were transformed to the standard system using observations of the Mark A field. For the near-IR data we used aperture photometry and used 2MASS stars in the field for photometric calibration. The zero-point uncertainties are of the order 0.03 mag for both the optical and near-IR bands.

The afterglow is not detected in the early MOA *RI*-band image, but it is clearly detected in the *BV*-image, which has a much lower sky background. We estimate an *R*-band magnitude by calibrating to internal *V* reference stars and assuming $V - R = 0.5$, the color determined on July 24.3.

In the left panel of Figure 1 we have plotted the *R*-band light curve ranging from 4.2 hr to 64 days after the XRF. Here we also show the tentative early unfiltered detections (2.7 and 3.1 σ) from the ROTSE-III Telescope (Smith et al. 2003a). The decay curve based on our data is consistent with being flat during the first 24 hr after the burst. Assuming that the ROTSE-III detections are real, they imply a declining phase during the first few hours. Around 1 day after the burst the decay slope steepens to about $\alpha = 2$ ($F_\nu \propto t^{-\alpha}$) and remains so for the following 4–5 days. About a week after the burst the light curve starts to deviate from its fast decay. It then quickly rises to a secondary maximum peaked at around 16 days, followed by another steep decline with power-law slope similar to that prior to the bump.

To quantify the properties of the early *R*-band light curve we have fitted a broken power law:

$$f_R(t) = \begin{cases} f_R(t_b)\left(\dfrac{t}{t_b}\right)^{-\alpha_1}, & \text{if } t \le t_b \\ f_R(t_b)\left(\dfrac{t}{t_b}\right)^{-\alpha_2}, & \text{if } t \ge t_b, \end{cases} \quad (1)$$

to the first 12 data points, up to 6 days past the burst. We find $\alpha_1 = 0.10 \pm 0.06$, $\alpha_2 = 1.84 \pm 0.04$, $t_b = 1.14 \pm 0.04$ days and $\chi^2 = 37$ for 7 degrees of freedom. Hence this functional form is formally rejected by the data. We then followed Beuermann et al. (1999) and fit an empirical function of the form

$$f_R(t) = [(k_1 t^{-\alpha_1})^{-n} + (k_2 t^{-\alpha_2})^{-n}]^{-1/n},$$

where t is the time since the XRF, measured in days. For large values of n this function approaches the broken power law, whereas small values provide a smoothly broken power law. We found that $n \approx 1.5$ gave the best fit. The decay slopes for $n = 1.5$ are $\alpha_1 = -0.08 \pm 0.08$ and $\alpha_2 = 2.15 \pm 0.08$ with $\chi^2 = 12$ for 7 degrees of freedom. In Figure 1 we have overplotted the two fits as a dotted (broken power law) and a solid (Beuermann) line.

3.3. *Spectral Energy Distribution*

The multiband observations of XRF 030723 allowed us to construct the spectral energy distribution (SED) at five epochs (July 24.4, July 25.4, July 27.2, August 6.3, and August 19.0 UT). The optical and near-IR magnitudes were corrected for Galactic reddening [$E(B - V) = 0.053$; Schlegel et al. 1998] and transformed to specific flux using the conversion factors given by Fukugita et al. (1995) and Allen (2000), respectively. Given that all multiband observations

TABLE 2
EVOLUTION OF THE XRF 030723 SED

Observing Epoch (UT)	Filters	β	χ^2/dof
Jul 24.4.....	$VRiJ_sHK_s$	0.96 ± 0.04	1.5
Jul 25.4.....	RJ_sHK_s	1.31 ± 0.13	3.6
Jul 27.2.....	$UBVRiJ_sHK_s$	1.00 ± 0.07	2.2
Aug 6.3	$BVRi$	1.03 ± 0.25	3.1
Aug 19.0	RiK_s	1.15 ± 0.10	58.3

were not performed exactly at the above mentioned five epochs, their corresponding fluxes were rescaled assuming a power-law decay ($F_\nu \propto t^{-\alpha}$). Based on the properties of the light curve, the assumed values for α were $\alpha = 2$ for July 24.4, July 25.4, July 27.2, and August 19.0 UT and $\alpha = 0$ for August 6.3 UT. In any case, the near-IR/optical magnitudes are well clustered around the aforementioned five epochs, so the final results are not strongly dependent on the assumed values of α. A power-law fit in the form $F_\nu \propto \nu^{-\beta}$ was carried out for the five epochs. The results are summarized in Table 2.

A power law provides a tolerable fit for the first four epochs. The spectral index is consistent with being constant with a value around $\beta \sim 1.0$. There is no indication of a significant spectral bend due to extinction as seen for, e.g., GRB 000301C (Jensen et al. 2001), GRB 000926 (Fynbo et al. 2001a; Price et al. 2001), or GRB 021004 (Holland et al. 2003). To constrain the amount of extinction we assumed an intrinsic power-law shape of the SED, an SMC-like extinction curve from Pei (1992), and a redshift in the range $z = 0.3$–1.0 (see § 4.2). For $z = 0.3$ the 2 σ upper limit on the rest frame A_V is 0.5 mag and for $z = 1.0$ the limit is 0.4 mag.

Unlike the earlier epochs, the August 19.0 UT SED shows a clear deviation from the power law (χ^2/dof = 58.3). Figure 2 shows the five epoch SEDs. The constraining *U*- and *B*-band upper limits of August 19.0 UT (see Fig. 2, *filled triangles*) indicate a clear deficit of flux at wavelengths shorter than ~5000 Å (observer frame) at this epoch.

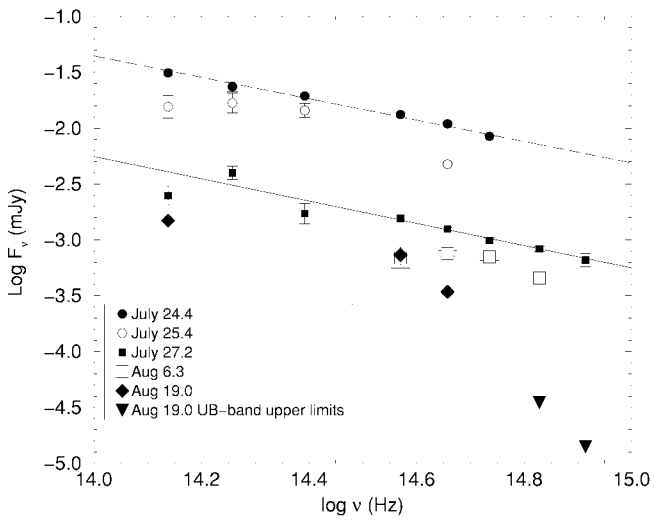

FIG. 2.—Evolution of the SED from July 24.4 to August 19.0. As seen, the SED is consistent with a power law in the first four epochs. However, after the bump in the light curve there is a strong deviation away from the power-law SED due to a faster drop in the bluest bands.

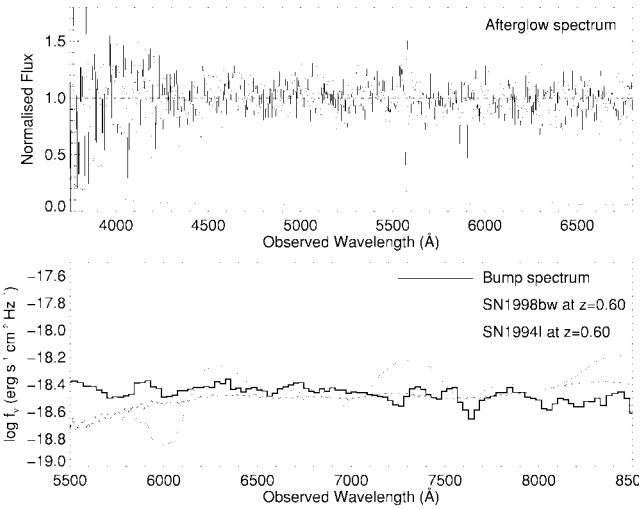

FIG. 3.—*Top:* The normalized spectrum of the optical afterglow from July 26.3. The dotted line shows the noise spectrum. There are no absorption lines significant at more than 2 σ. We show only the spectral region from 3750 Å to 6800 Å that is largely unaffected by strong sky-subtraction residuals. *Bottom:* The solid line shows the spectrum of XRF 030723 taken during the peak of the light-curve bump (August 7.4–8.4). The spectrum has been rebinned in 30 Å wide wavelength bins. For comparison we show the spectra of SN 1998bw (taken at 3 days past *B*-band peak; Patat et al. 2001) and SN 1994I (taken 1 day past *B*-band peak; Clocchiatti et al. 1996). Both spectra have been redshifted to $z = 0.6$ (see § 4.3) and scaled in flux to match the level of the bump spectrum. The spectrum of the bump is compatible with that of a SN with a high expansion velocity similar to SN 1998bw or SN 2002ap, while we can probably exclude a SN with a low expansion velocity (as SN 1994I).

3.4. *Spectroscopy*

Spectra of the source were obtained with the VLT on three epochs (see Table 1). A 13.2 ks spectrum was obtained on July 26.3 when the afterglow had a magnitude of $V \approx 23.3$. We used the 300V grism with the GG375 order separation filter and a 1.″0 wide slit providing a resolution of 13.3 Å over the spectral region from 3800 to 8900 Å. The spectrum shows a featureless continuum with no strong (larger than 3 σ) absorption or emission lines superposed. The normalized spectrum is shown in the upper panel of Figure 3.

We also secured spectra of the afterglow at the phase of the light-curve bump. This was complicated by the bright Moon, which was located near the field of XRF 030723 on the sky around the time of the bump. The spectra were secured on August 7.4 and 8.4 with a total integration time of 13.5 ks. These spectra were obtained with the 600RI grism and the GG435 order separation filter and a 1.″0 wide slit providing a spectral coverage of 5300–8600 Å with a resolution of 6.6 Å. The spectrum shows a faint continuum with no narrow absorption or emission lines detected above 3 σ significance (Fig. 3). This spectrum is consistent with the broadband photometry from August 6.3.

3.5. *The Host Galaxy*

In our latest *R*-band image from September 25.1 there is a faint, extended source with magnitude $R = 26.8 \pm 0.4$ at the position of the afterglow (Fig. 4 and Fynbo et al. 2003). However, a deeper and later image taken with the SUBARU Telescope shows the presence of a $R = 27.6 \pm 0.4$ point source at the afterglow position (Kawai et al. 2003). The nearest other galaxy is located about 2″ north of the position of the afterglow. While we cannot exclude this

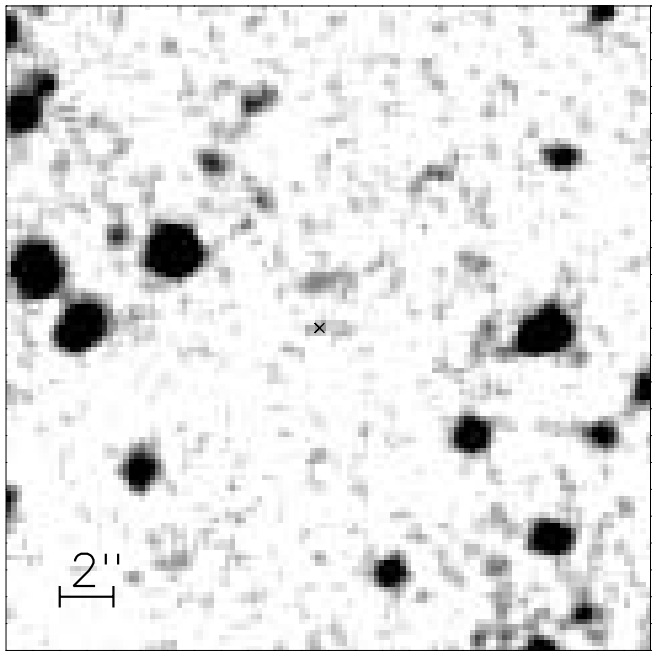

FIG. 4.—The 24×24 arcsec^2 field around the position of XRF 030723 from our latest VLT R-band image 64 days after the burst. East is to the left, and north is up. The position of the afterglow is marked with a cross (the size of the cross corresponds to the 10 σ error circle on the astrometry). There is some evidence for an extended source with position angle about 90° (east of north) at the position of the afterglow (Fynbo et al. 2003). However, a later and deeper SUBARU image shows only a fainter point source at the afterglow position (Kawai et al. 2003). Further deep imaging is required to reveal the nature of the host galaxy.

object as the host galaxy, it is most likely unrelated to XRF 030723. We therefore consider $R \approx 27$ to be an upper limit on the magnitude of the host galaxy of XRF 030723. Further deep imaging is required to reveal the nature of the host galaxy.

4. DISCUSSION

4.1. *The Afterglow*

This study of XRF 030723 is the first example of an XRF optical afterglow that has been extensively monitored. The properties of the early light curve and SED are consistent with the hypothesis that XRFs are due to the same phenomenon as classical GRBs, but seen at a larger viewing angle. In this scenario the early light curve is the result of the competition between two effects: (1) the decrease in observed flux from the afterglow with time as for normal on-axis GRBs and (2) an increase in flux from the afterglow as more and more of the jet becomes visible to the observer with time. The combination of these effects results in a flatter early light curve than for GRB afterglows and even a rising early light curve for some viewing angles (see Granot et al. 2002; Rossi et al. 2002; see Dado et al. 2003 for a discussion in the case of fireball and cannonball models). In addition, the shape of the jet may be important. In the collapsar model there is more slowly moving material further away from the jet axis, and the early optical afterglow from an XRF will be dominated by emission from this material (Zhang et al. 2004; Kouveliotou et al. 2004). The exact shape of the early light curve will hence be a function of the jet structure, the viewing angle, and the density profile of the environment. It is possible to reconcile the tentative ROTSE-III detection with the off-axis scenario in the following way: The steep decline following the constant phase indicate that this radiation comes from material that is off-axis, i.e., our line of sight is outside the range of angles in which this material flows out. The decay rate during the ROTSE observations is poorly constrained, but a steep decay, approximately t^{-2}, is most consistent with our first data point. That means that this material, too, is viewed off-axis, and very likely it is the same material that caused the off-axis prompt emission to which we attribute the XRF. Because the strength of off-axis emission decreases very steeply with angle away from the axis, this suggests that our line of sight is not too far outside the opening angle of the fast material that made the prompt emission. That then does not leave much solid angle for the slower material that caused the plateau. The time of its break, about 1 day after trigger, implies an opening angle of about 10° for explosion energies and external densities typical of ordinary GRBs, and a minimum initial Lorentz factor of 5–10 for this material. Its total energy must be larger than that of the faster material in order to cause the strong reflare responsible for the flat light curve. It is important to note that for this interpretation it is not required that the slower material be further off-axis than the fast material: it could also occupy the same cone, but follow behind the fast material and cause a reenergizing of the original forward shock.

We note that flat light curves have been seen also for a few classical GRBs. The optical afterglow of GRB 970508 was almost constant from 3 to 24 hr after the burst. It then rose by about 1 mag before it entered the usual power-law decline (Pedersen et al. 1998). Panaitescu & Kumar (2002) interpret this light curve as the result of a slightly off-axis GRB. The ROTSE-III observations of the optical afterglow of GRB 030418 showed a rise during the first 600 s and a roughly constant level during the following 1400 s (Smith et al. 2003b). Finally, we note that the light curve of GRB 000301C displayed a flat light curve 3–4 days after the GRB (Jensen et al. 2001).

The late afterglow light curve, i.e., from 1 to 5–6 days after the burst, is also as expected for off-axis GRBs. The value $\alpha_2 \sim 2$ is the canonical late time slope (see, e.g., Andersen et al. 2000, their Fig. 4.) reflecting the slope of the distribution of energies for relativistic electrons producing the afterglow emission in the synchrotron model (e.g., van Paradijs et al. 2000). Finally, the spectral slope of $\beta \approx 1.0$ is also typical for GRB afterglows (e.g., Simon et al. 2001).

The afterglow of XRF 030723 has also been detected in the X-ray band with the *Chandra X-Ray Telescope* on July 25 and August 4 (Butler et al. 2004). The properties of the X-ray afterglow is within the range of classical GRBs. The decline of the X-ray afterglow from July 25 to August 4 corresponds to a power-law decay slope of $\alpha_X = 1.0 \pm 0.1$ (Butler et al. 2004). This is slower than the optical decay suggesting either a nontrivial behavior of the afterglow or that the bump could also be present in the X-ray light curve. For a full discussion of X-ray emission from GRBs, XRFs, and supernovae (SNe) we refer the reader to Kouveliotou et al. (2004).

4.2. *Limits on the Redshift*

We first discuss which limits we can place on the redshift from the afterglow spectrum. The lack of Lyα absorption down to 4000 Å due to H I in the intergalactic medium (the Lyα forest), allows us to infer a firm upper limit of $z \leq 2.3$ for the redshift of XRF 030723. It should be noted that this is the first time a firm redshift limit can be set from an XRF afterglow spectrum—and that this has led to the firm conclusion

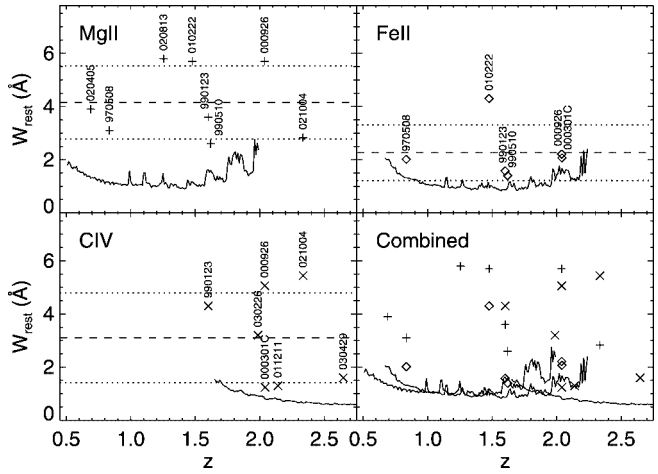

FIG. 5.—Upper limit on the rest-frame equivalent width as a function of redshift. In the three panels labeled Mg II, Fe II, and C IV we present the 2 σ upper limits (*solid lines*) on the total $W_{\rm rest}$ measured in the afterglow spectrum as a function of assumed redshift for the mentioned transitions. The upper limits are compared to GRBs with known Mg II (*plotted with plus signs*), Fe II (*open diamonds*) and C IV (*crosses*) equivalent widths. The dashed and dotted lines show the mean and 1 σ spread of the $W_{\rm rest}$ GRB measurements. The lower right panel shows the combined plot of the three other panels.

that this XRF is not simply a high-redshift GRB. If we would furthermore make the assumption that the absorption system associated with the host galaxy of XRF 030723 has properties similar to those of GRB absorption systems, we can place stronger limits on the redshift. The 1 σ observed equivalent width ($W_{\rm obs}$) for absorption lines over the region 4000–6400 Å is about 1 Å. This is the region where the signal-to-noise ratio in the spectrum is highest and the spectrum is not affected by strong sky-subtraction residuals. GRB absorption systems appear to always have strong Lyα absorption lines (Jensen et al. 2001; Fynbo et al. 2001b; Møller et al. 2002; Hjorth et al. 2003b; Vreeswijk et al. 2004). From the lack of Lyα absorption an upper limit of $z = 2.1$ can be inferred. GRB absorbers also show C IV absorption lines at 1548/1550 Å with rest equivalent width ($W_{\rm rest}$) in the range 1.2–5.1 Å (see the same references as for Lyα). Therefore a C IV line should have been detected at more than 3 σ significance if the redshift is larger than $z = 1.6$. Furthermore, the Mg II doublet at 2800 Å has a total $W_{\rm rest}$ in the range 2.6–12 Å for GRB absorption systems (e.g., Metzger et al. 1997; Andersen et al. 1999; Vreeswijk et al. 2001; Jensen et al. 2001; Castro et al. 2003; Jha et al. 2001). The absence of Mg II absorption would exclude the redshift range $0.4 < z < 1.4$ under the assumption of absorption lines similar to GRB absorbers.

We have performed a cross-correlation between the observed afterglow spectrum and a simulated spectrum containing only absorption from Fe II and Mg II, but this cross-correlation did not reveal any significant peaks. Because of the lack of redshift information we turned to the following method. Assuming a redshift, we used the spectrum to measure the variance within one resolution element at the expected position of a feature. By doing this for a sequence of redshifts we can plot the 2 σ upper limit on $W_{\rm rest}$ for Mg II, Fe II, and C IV. For Fe II we only used the two strongest features, Fe II λ2382 and λ2600. The upper limits are compared to known equivalent widths of GRBs in Figure 5. The figure shows that if the absorption lines from the absorption system associated with XRF 030723 had been similar to the absorbers associated with known GRBs, we would have expected an absorption line from either Mg II, Fe II, or C IV if the redshift is larger than $z = 0.5$.

However, if at $z < 0.5$ the host galaxy is extremely faint. Bloom et al. (2003) argued that two XRF hosts were at $z > 0.6$ based on their luminosities, and the host of XRF 030723 is almost 3 mag fainter than these hosts. In fact, at $z < 0.5$ the host galaxy has to be fainter than $M \approx -15$. We therefore consider this low-redshift unlikely.

It is more plausible that the absorption system associated with XRF 030723 is weaker than typically found for GRB absorbers. This would imply that XRF 030723 is located in an environment with lower density than found for most GRBs so far. We consider the upper limit of $z < 2.3$ the only strong limit we have on the redshift of XRF 030723 based on the afterglow spectrum.

Finally, we note that Atteia et al. (2004) have determined fiducial redshifts (pseudo-z) for a sample of *HETE* bursts. The pseudo-z is based on the high-energy properties of the burst. For XRF 030723 Atteia et al. report a pseudo-z of 0.59.

4.3. *The Nature of the Bump*

For long-duration GRBs the relation to SNe became firmly established with the discovery of the Type Ic supernova SN 2003dh associated with GRB 030329 (Stanek et al. 2003; Hjorth et al. 2003a). If XRFs are simply the same phenomenon as long-duration GRBs but seen further away from the jet axis, we would also expect to see supernovae underlying the light curves of XRFs. It would thus be natural to try to explain the bump we see in Figure 1 as the signature of a SN. The putative supernova peaks after about 16 days in the R band, and the spectral energy distribution after the peak becomes significantly redder than the early power-law spectra (see § 3.3). This motivates us to investigate whether the bump is consistent with a supernova origin, in terms of peak luminosity, timing, and SED.

The peak time of approximately 16 days after the XRF is early even for a local supernova. The light-curve peak is also unusually narrow. Fitting a simple Gaussian to the peak gives a value of 1.7 mag for Δm_{15}, i.e., the increase in magnitude between peak and 15 days later. Correcting for time dilation corresponding to a reasonable redshift, the intrinsic width gets even smaller (and Δm_{15} larger). Early, narrow SN light-curve peaks are expected from progenitor stars that have lost (most of) their hydrogen (and helium) envelopes. Of the known supernovae, the one we have found to produce the best match to the light curve is the Type Ic SN 1994I. In the right panel of Figure 1 we plot the B-band light curve of SN 1994I redshifted to $z = 0.6$ on top of the light curve of XRF 030723. We have subtracted an extrapolation of the power-law afterglow component (from the Beuermann fit). The errors include the photometric error as well as the formal error from the subtraction of the Beuermann fit. As seen, the match is qualitatively acceptable except for data points before the peak. We cannot, however, exclude an afterglow light-curve shape that is different from the purely empirical Beuermann function. Such a difference would give large systematic errors on the data point prior to the peak. In particular, a steeper late time decay slope would leave more room for a longer rise time for the SN. SN 1994I displayed a very fast light curve (Richmond et al. 1996). Further, the observations of SN 1994I show that the peak width becomes narrower at shorter wavelengths, so a near-UV light curve will surely be intrinsically more narrow than a B-band light curve, partially canceling the time dilation

effect. In addition, the decline rate, as measured by Δm_{15}, also differs considerably between different Type Ic supernovae. Richmond et al. (1996) estimate for SN 1994I that $\Delta m_{15}(U) \sim 2.5$ (our estimate), $\Delta m_{15}(B) \sim 2.1$, and $\Delta m_{15}(V) \sim 1.7$, while the peak magnitude was reached after 8, 9, and 10 days ($\tau_{\rm peak}$), in the U, B, and V bands, respectively. For SN 1998bw we estimate the corresponding numbers from Galama et al. (1998) to be $\Delta m_{15}(U) \sim 1.3$, $\Delta m_{15}(B) \sim 1.0$, $\Delta m_{15}(V) \sim 0.7$, and $\tau_{\rm peak}(U) = 13.5$, $\tau_{\rm peak}(B) = 14.7$, and $\tau_{\rm peak}(V) = 17.0$ days. Finally, SN 2002ap reached maximum brightness in U at 6.2 days, and in V at 9.9 days (Foley et al. 2003). There is thus a large variation in both the rise time and decay time of Type Ic supernovae. It is, however, obvious that any supernova connected to XRF 030723 has to have a light curve which is at least as fast as SN 1994I, and quite unlike SN 1998bw.

Although SN 1994I is the fastest Type Ic to date, there is no reason to exclude even faster scenarios. In a simple model, the width of the light curve at the peak is set by $\tau_{\rm peak} \propto \kappa^{1/2} M^{3/4} E^{-1/4}$ (e.g., Arnett 1996), where E is the total energy, M the mass of the ejecta, and κ the opacity. A faster light curve could therefore imply a smaller ejecta mass or/and a more energetic explosion. A lower effective opacity, caused by, e.g., a higher effective temperature, would also decrease $\tau_{\rm peak}$. Because the estimated C—O core mass of SN 1994I is only $\sim$2.1 $M_\odot$ (Iwamoto et al. 1994), the most likely reason for a faster timescale is a higher kinetic energy, possibly in combination with a large asymmetry. As several studies have shown (e.g., Maeda & Nomoto 2003; Woosley & Heger 2003), a highly asymmetric explosion may result in a fast rise time. A less central distribution of the radioactive ^{56}Ni would further enhance this effect. Because the diffusion time $\tau_d \propto R^2 \rho \kappa \propto 1/(Vt)$, faster expansion in the polar direction leads to a shorter τ_d and a faster rise time (Höflich et al. 1999).

The absolute magnitude at the peak is determined by the amount of ejected ^{56}Ni, which is not necessarily correlated with the parameters determining the width of the peak. The late bump of XRF 030723 peaked at $R \approx 24.0$. This may provide a hint as to the redshift for the object. At a redshift of $z = 0.4$, the apparent supernova bump would be as faint as SN 1994I. While the putative supernova could in principle be even fainter than the mediocre SN 1994I, even lower redshifts would also make the host an unusually faint galaxy (see § 4.2). On the other hand, for a redshift of $z = 1.0$, the assumed bump would correspond to a supernova about 3 times as bright as the powerful SN 1998bw.

There is not much information from the SED (Fig. 2) to confirm a supernova origin for the late bump. However, the clear red evolution of the SED can exclude many other possible origins (see below). If the redshift is as high as $z \sim 1$, most of the observed optical emission (*UBVRI*) will correspond to the near-UV regime, which is poorly known for Type Ib/c supernovae at early phases. An *HST* spectrum of SN 1994I does show a strong depression in the UV at 11 days past B maximum (Millard et al. 1999). This is also seen in Type Ia and Type IIP supernovae, and it is interpreted as arising from the strong UV blanketing due to the abundance of overlapping lines from especially Ca II, Fe I, and Fe II, as well as bound-free absorption by C II. The only really early near-UV spectrum of a Type Ic supernova we are aware of is a *HST* spectrum of SN 2002ap taken 6 days before maximum (courtesy of the SINS-team, PI: Kirshner). This spectrum also shows a steep decline into the UV. The flux decreases by a factor of 10 between 4300 to 2700 Å.

We stress, however, that a comparison with the very limited local sample of Type Ic supernovae may be misleading for several reasons. It is quite likely that the X-ray flash emerges in the polar direction, where the expansion velocities are highest and the density lowest. These parts of the ejecta may also have a higher ^{56}Ni fraction, and therefore a higher effective temperature. These factors may together lead to a higher degree of ionization at these stages, which would make UV line blanketing less effective. A measurable UV flux at the time of the peak—as would be needed to interpret the light-curve bump as due to a supernova at $z \sim 1$, could therefore result.

If we interpret the nondetections in the *UB* bands after the peak as due to the UV-blanketing, the redshift would have to be in the range $z \sim 0.3$–1.0. The late K-band detection also argues against a lower redshift, to match the SED of known Type Ic supernovae (e.g., Yoshii et al. 2003).

The absence of any supernova features in the spectrum taken in the bump phase is not surprising since the expected small-amplitude undulations in this limited wavelength range are not likely to stand out at this signal-to-noise ratio (see Fig. 3). This is true for SNe with large expansion velocities like SN 1998bw. We can, however, probably exclude SNe with lower expansion velocities, as for SN 1994I (see Fig. 3). Very broad spectral features, and a narrow light curve, are expected from an energetic and asymmetric explosion viewed pole on (e.g., Iwamoto et al. 1998; Höflich et al. 1999).

In summary, an interpretation of the late, red light-curve bump as due to a supernova at redshift $z = 0.3$–1.0 appears to be consistent with the observations. This fits nicely with the recent findings of a firm supernova connection for GRB 030329 (Garnavich et al. 2003; Stanek et al. 2003; Hjorth et al. 2003a) and with the spectroscopic redshift ($z = 0.25$) of the probable host of XRF 020903 (Soderberg et al. 2003b). Regarding the SED we can only qualitatively say that the SED is consistent with a supernova that is emitting strongly in the UV at maximum, but for which the UV-depression sets in at later phases. A more secure and quantitative statement is prevented by the poor knowledge of the early UV spectra of Type Ic supernovae and the lack of a spectroscopic redshift.

Other explanations to consider for the bump are (1) a refreshed shock (Granot et al. 2003 and references therein), (2) a two-jet model like the one proposed for GRB 030329 (Berger et al. 2003; Huang et al. 2004), (3) the encounter with the termination shock of the progenitor wind or other density enhancements (e.g., Ramirez-Ruiz et al. 2001), (4) a dust-echo (Esin & Blandford 2000; Reichart 2001), and possibly (5) microlensing (Garnavich et al. 2000). The sharp rise of the light curve in the bump phase is difficult to explain for density variations or refreshed shocks. The light curve can be reasonably well described by a two-jet model (Huang et al. 2004). However, the fundamental problem with most of the alternative models is to explain the SED. A power-law SED is expected at all epochs, and this is clearly excluded by the data. On the other hand, an increasing absorption of blue light is probably a generic feature for a supernova. We find the dust echo unlikely as the host appears to be a tiny dwarf galaxy that most likely has a very low dust content. Therefore, we consider a SN the most likely explanation for the late light-curve bump. Within this scenario, the evolution of the X-ray afterglow remains to be fully understood.

5. CONCLUSIONS

We have presented the first detailed multicolor study of the afterglow of an XRF. The properties of the early light curve

are in agreement with the predictions for off-axis classical GRBs both in the fireball and cannonball models. After the first week there is a strong bump in the light curve, peaking at around 16 days after the XRF. The SED after the peak of the bump becomes significantly redder and can no longer be fitted by a power law. We have considered the possible interpretations of this bump, e.g., an underlying supernova, a second jet, a refreshed shock or an encounter with a density enhancement. We conclude that a SN is the most likely explanation since no other model can qualitatively explain the evolution of the SED. We also present deep spectroscopy of the burst both in the afterglow and in the bump phase. Unfortunately, no redshift determination has resulted from the spectra as there are no significant absorption or emission lines detected. A firm upper limit of $z \leq 2.3$ on the redshift is established from the lack of any Lyα forest lines in the afterglow spectrum. If the bump in the light curve is indeed due to a supernova the most likely redshift is in the range $\sim$0.3–1.0. The lack of significant absorption lines in the afterglow spectrum and the lack of any indication of extinction in the afterglow SED is indicative that the progenitor was in an environment with lower density than typically found for GRBs. The host galaxy has not been unambiguously detected. From the upper limit of $R \gtrsim 27.0$ and the preferred redshift range of $z \approx 0.3$–1.0 we conclude that the host is a dwarf galaxy.

This paper is based on observations collected by the Gamma-Ray Burst Collaboration at ESO (GRACE) at the European Southern Observatory, Paranal, and La Silla, Chile. We thank the ESO staff for their help in securing the service mode data reported here. This publication makes use of data products from the Two Micron All Sky Survey, which is a joint project of the University of Massachusetts and the Infrared Processing and Analysis Center/California Institute of Technology, funded by the National Aeronautics and Space Administration and the National Science Foundation. The allocation of observing time by IJAF at the Danish 1.54 m telescope on La Silla is acknowledged. A. J. Castro-Tirado acknowledges the time devoted to the GRB target of opportunity program within the MOA Project at Mount John. We acknowledge benefits from collaboration within the EU FP5 Research Training Network "Gamma-Ray Bursts: An Enigma and a Tool." This work was also supported by the Danish Natural Science Research Council (SNF) and by the Carlsberg Foundation.

REFERENCES

Allen, C. W. 2000, Allen's Astrophysical Quantities ed. A. N. Cox (4th ed; New York: Springer)
Amati, L., et al. 2002, A&A, 390, 81
Andersen, M. I., et al. 1999, Science, 283, 2075
———. 2000, A&A, 364, L54
Arnett, W. D. 1996, Supernovae and Nucleosynthesis (Princeton: Princeton Univ. Press)
Atteia, J.-L., et al. 2004, preprint (astro-ph/0312371)
Band, D., et al. 1993, ApJ, 413, 281
Barraud, C., et al. 2003, A&A, 400, 1021
Berger, E., et al. 2003, Nature, 426, 154
Beuermann, K., et al. 1999, A&A, 352, L26
Bloom, J. S., et al. 2003, ApJ, 599, 957
Butler, N., et al. 2004, preprint (astro-ph/0401020)
Castro, S., et al. 2003, ApJ, 586, 128
Castro-Tirado, A. J., et al. 1994, in AIP Conf. Proc. 404, Gamma-Ray Bursts, ed. Fishman, G. J., Brainerd, J. J., & Hurley, K. H. (New York: AIP), 17
Clocchiatti, A., Wheeler, J. C., Brotherton, M. S., Cochran, A. L., Wills, D., Barker, E. S., & Turatto, M. 1996, ApJ, 462, 462
Dado, S., Dar, A., & de Rújula, A. 2003, A&A, in press (astro-ph/0309294)
Dermer, C. D., Chiang, J., & Böttcher, M. 1999, ApJ, 513, 656
Esin, A. A., & Blandford, R. 2000, ApJ, 534, L151
Foley, R. J., et al. 2003, PASP, 115, 1220
Fox, D. B. 2002, GCN 1387
Fox, D. B., Kaplan, D. L., Kulkarni, S. R., & Nechita, A. 2003, GCN 2323
Frail, D. A. 2003, GCN 2473
Fukugita, M., Shimasaku, K., & Ichikawa, T. 1995, PASP, 107, 945
Fynbo, J. P. U., et al. 2001a, A&A, 373, 796
———. 2001b, in Proc. MPA/ESO/MPE/USM Joint Astronomy Conf., Lighthouses of the Universe: The Most Luminous Celestial Objects and Their Use for Cosmology, ed. M. Gilfanov, R. Sunyaev, & E. Churazov (Garching: Springer), 187
———. 2003, GCN 2403
Galama, T. J., et al. 1998, Nature, 395, 670
Garnavich, P., Loeb, A., & Stanek, K. Z. 2000, ApJ, 544, 11
Garnavich, P., Matheson, T., Olszewski, E. W., Harding, P., & Stanek, K. Z. 2003, IAU Circ. 8114
Granot, J., Nakar, E., & Piran, T. 2003, Nature, 426, 138
Granot, J., Panaitescu, A., Kumar, P., & Woosley, S. E. 2002, ApJ, 570, L61
Harrison, F. A., et al. 2001, GCN 1143
Heise, J., in 't Zand, J., & Kippen, R. M. 2003, in AIP Conf. Proc. 662, Gamma-Ray Bursts and Afterglow Astronomy, ed.G . R. Ricker & R. K. Vanderspek (Melville: AIP), 229
Heise, J., in 't Zand, J., Kippen, R. M., & Woods, P. M. 2001, in Gamma-ray Bursts in the Afterglow Era ed. E. Costa & F. Frontera (Berlin: Springer), 16
Hjorth, J., et al. 2003a, Nature, 423, 847
———. 2003b, ApJ, 597, 699
Holland, S. T., et al. 2003, AJ, 125, 2291
Huang, Y. F., Wu, X. F., Dai, Z. G., Ma, H. T., & Lu, T. 2004, ApJ, 605, 300
Höflich, P., Wheeler, J. C., & Wang, L. 1999, ApJ, 521, 179
Iwamoto, K., et al. 1994, ApJ, 437, 115
———. 1998, Nature, 395, 672
Jensen, B. L., et al. 2001, A&A, 370, 909
———. 2003, GCN 2321
Jha, S., et al. 2001, ApJ, 554, L155
Kawai, N., et al. 2003, GCN 2412
Kippen, R. M., et al. 2002, in AIP Conf. Proc. 662, Gamma-Ray Bursts and Afterglow Astronomy, ed. G. R. Ricker & R. K. Vanderspek (Melville: AIP), 244
Kouveliotou, C., et al. 2004, ApJ, 608, 872
Lamb, D. Q., Donaghy, T. Q., & Graziani C. 2003, ApJ, submitted (astro-ph/0312634)
Levan, A., et al. 2002, GCN 1761
Maeda, K. & Nomoto, K. 2003, ApJ, 598, 1163
Metzger, M. R., et al. 1997, Nature, 387, 879
Millard, J., et al. 1999, ApJ, 527, 746
Møller, P., et al. 2002, A&A, 396, L21
Nemiroff, R. J., et al. 1994, ApJ, 435, L121
Panaitescu, A., & Kumar, P. 2002, ApJ, 571, 779
Patat, F., et al. 2001, ApJ, 555, 900
Pedersen, H., et al. 1998, ApJ, 496, 311
Pei, Y. C. 1992, ApJ, 395, 130
Preece, R. D., Mallozzi, R. S., Pendleton, G. N., & Paciesas W. S. 2000, ApJS, 126, 19
Price, P. A., et al. 2001, ApJ, 549, L7
Prigozhin, G., et al. 2003, GCN 2313
Prochaska, J. S., et al. 2004, ApJ, submitted (astro-ph/0402085)
Ramirez-Ruiz, E., Dray, L. M., Madau, P., & Tout, C. A. 2001, MNRAS, 327, 829
Reichart, D. E. 2001, ApJ, 554, 643
Rhoads, J. E. 2003, ApJ, 591, 1097
Richmond, M. W., et al. 1996, AJ, 111, 327
Ricker, G., et al. 2002, GCN 1530
Rossi, E., Lazzati, D., & Rees, M. J. 2002, MNRAS, 332, 945
Schlegel, D. J., Finkbeiner, D. P., & Davis, M. 1998, ApJ, 500, 525
Simon, V., Hudec, R., Pizzichini, G., & Masetti, N. 2001, A&A, 377, 450
Smith, D. A, Akerlof C. W., & Quimby R. 2003a, GCN 2338
Smith, D. A., et al. 2003b, BAAS, 203, 132.01
Soderberg, A. M., Berger, E., & Frail, D. A. 2003, GCN 2330
Soderberg, A. M., et al. 2003, AAS Meeting, 203, 132.07

Stanek, K. Z., et al. 2003, ApJ, 591, L17
Stetson, P. B. 1987, PASP, 99, 191
———. 1994, PASP, 106, 250
Taylor, G. B., et al. 2001, GCN 1136
van Dokkum, P. G., & Bloom, J. S. 2003, GCN 2380
van Paradijs, J., Kouveliotou, C., & Wijers, R. A. M. J. 2000, ARA&A, 38, 379
Vaughan, S., et al. 2004, ApJ, 603, L5
Vreeswijk, P. M., et al. 2001, ApJ, 546, 672
Vreeswijk, P. M., et al. 2004, A&A, in press (astro-ph/0403080)
Watson, D., et al. 2004, ApJ, 605, L101
Woosley, S. E., & Heger, A. 2003, ApJ, submitted (astro-ph/0309165)
Yamazaki, R., Ioka, K., & Nakamura, T. 2002, ApJ, 571, L31
———. 2003, ApJ, 593, 941
Yoshii, Y., et al. 2003, ApJ, 592, 467
Zhang, B., & Mészáros, P. 2002, ApJ, 581, 1236
Zhang, W., Woosley, S. E., & Heger, A. 2004, ApJ, 608, 365